

Mitigating Multimodal Hallucinations via Gradient-based Self-Reflection

Shan Wang
NVIDIA

Maying Shen
NVIDIA

Nadine Chang
NVIDIA

Chuong Nguyen
Data61, CSIRO

Hongdong Li
Australian National University

Jose M. Alvarez
NVIDIA

Abstract

Hallucinations in multimodal large language model are caused by the text-visual bias and the co-occurrence bias. The former reflects an over-reliance on text information in the decision-making process, while the latter arises from the statistical object-pairing patterns abstracted from the training data. Existing mitigation methods heuristically address these biases without understanding the fluctuating bias level across the instances. We first propose estimating the influence of respective token types (visual, prompt, and previous outputs) using a gradient-based self-reflection method. The estimated token influence further enables the detection of object-related visual tokens and their integration into an influence-aware contrastive decoding framework to mitigate both types of biases simultaneously. Our method operates without the need for additional resources, such as costly fine-tuning, extra models, or data statistics. Extensive experiments show it effectively reduces hallucinations, achieving up to a 92% accuracy increase on LLaVA-QA90.

1 Introduction

Multimodal Large Language Models (MLLMs) [31, 9, 47, 2, 6], have recently gained significant momentum in generating coherent, context-aware content across diverse domains. Despite their impressive capabilities, these models face a significant challenge: hallucination, where the generated text content is not grounded in the visual inputs [40, 29]. This issue undermines the trust in the outputs of MLLMs.

Hallucinations in MLLMs are found to arise from two key biases studied in the literature [29, 20, 23]: text-visual bias, and co-occurrence bias. **Text-visual bias** arises when a model relies too heavily on textual input, and neglects the visual information. This bias is also linked to the generated text length [54, 12]. Longer text increases the risk of hallucinations, often stemming from early predictions that overly influence subsequent content generation. **Co-occurrence bias** arises from statistical correlations in the training data [29], causing models

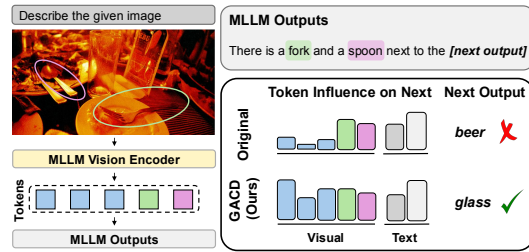


Figure 1: Overview of our method, which acts as a token-wise post-processing mechanism to mitigate text-visual hallucinations by enhancing visual influence (colored bars) in prediction. Our token-influence approach explicitly aligns this amplification with the most influential text inputs—either prompts (gray bar) or previous outputs (white bar). By leveraging token-wise influence measurement, the method also mitigates co-occurrence bias by selectively avoiding the enhancement of visual tokens (green and magenta bars) linked to previously mentioned objects.

to incorrectly predict objects based on their frequent pairings even when those objects are absent from the visual input. This bias is challenging to address, and currently lacks mitigation solutions that are free from statistical awareness.

Inference-based hallucination mitigation methods [26, 5] receive more attention than training-based approaches [7, 18, 50, 3, 42, 20] due to their cost effectiveness, as they eliminate the necessity for data collection, statistical analysis, and model training. Existing inference-related methods [26, 38, 12, 45] mitigate hallucination heuristically but lack a clear understanding of bias severity. Among inference-related methods, revision approaches [46, 10, 39] often require additional models for prediction validation, such as MLLM-based scoring, which may also hallucinate. Meanwhile, image-level methods [26, 12, 53] fail to address co-occurrence hallucinations at the token (individual object) level. Existing token-level approaches [45, 19, 5] either lack semantic awareness of visual tokens or rely on auxiliary segmentation or detection models to obtain decoupled visual representations. Therefore, a method that jointly and quantitatively addresses all biases without requiring additional data, or models remains a challenging and unresolved issue.

In this work, to quantitatively estimate biases, we introduce a gradient-based **token influence**, which leverages the first-order Taylor expansion [41] to estimate how each input token influences the output. This token influence enables the detection of the corresponding visual token of each predicted object (noun). In addition, we incorporate both token influence and the detected object-related visual tokens into a contrastive decoding framework [28] and propose Gradient-based Influence-Aware Contrastive Decoding (GACD) to jointly mitigate text-visual and co-occurrence biases. To address text-visual bias, GACD enhances visual token influence, aligning it with the most influential text components from prompts or previous outputs. This ensures visual grounding answer and prevents visual forgetting. To mitigate the co-occurrence bias, GACD selectively avoids enhancing visual tokens linked to objects mentioned in previous outputs. As illustrated in Fig. 1, GACD corrects the hallucinated prediction of ‘beer’ by enhancing the influence of visual tokens unrelated to ‘fork’ or ‘spoon’, resulting in a more visually grounded output. As text-visual bias tends to occur in long sentence generation [54], we further introduce a sample-dependent stopping criterion based on visual influence to explicitly capture visual contributions and account for length effects.

Contributions of this work is summarized as:

- We propose GACD, a novel hallucination mitigation method that reduces text-visual bias by enhancing the influence of visual tokens, without requiring external models or fine-tuning. Its token-wise adjustment further enables the mitigation of co-occurrence bias without relying on training dataset statistics.
- We propose token influence to express MLLM biases, providing a detailed understanding at both the token (individual object) level and the sample level.
- Extensive experiments demonstrate that GACD effectively mitigates hallucinations and enhances accuracy without sacrificing information. GACD achieves up to 8% increase in overall score on AMBER [44], an 8% F1 boost on POPE [29], up to 45% improvement in detailness and a 92% accuracy gain on LLaVA-QA90 [32].

2 Related Work

Hallucination and Bias. Hallucinations in LLMs often arise from biases in the training data [37, 16], while in MLLMs, studies [43, 29, 13] show that hallucinations are closely linked to biases like text-visual and co-occurrence biases. Additionally, biases related to output position, which increase the risk of hallucination as output length grows, have been examined in [12, 54]. Existing methods [29, 13, 23] typically report only overall statistics, lacking a mathematical, sample-wise bias measurement. This distinction is important, as biases can vary case by case. Our approach measures sample-dependent bias via token-level gradient sensitivities, revealing how pre-trained MLLM parameters embed these biases [22, 15], and enabling self-reflective hallucination mitigation.

Hallucination Mitigation. Training-related hallucination mitigation methods [4, 18, 50, 3, 42, 24] are expensive, requiring access to training data and specialized statistical analysis to effectively mitigate hallucinations. Reinforcement-learning approaches [36, 46, 10, 39, 51] rely on supplementary feedback, often from human annotators or auxiliary LLMs/MLLMs, and the latter may themselves hallucinate. By contrast, post-decoding techniques modify model logits at inference time without

further training or external feedback, making them lightweight add-ons. In text-only LLMs, such methods aim to align outputs with factual knowledge [8, 25, 27]. In MLLMs, post-decoding strategies emphasize the role of visual inputs [27, 26, 53, 12] and can be classified into image-level and token-level interventions. Image-level decoding methods [26, 53, 12, 52, 35] treat all objects in the input image uniformly, limiting their effectiveness in addressing co-occurrence hallucinations. Existing token-level methods either rely on external segmentation [5] and detection models [19] or lack awareness of object-related decoupling [45]. In contrast, our method estimates embedded bias and decouples object-aware visual tokens, enabling comprehensive and sample-specific hallucination mitigation without relying on external data or models.

3 Method

In this section, we provide background on MLLMs, introduce the concept of token influence, and explain how GACD balances token influence through contrastive decoding to mitigate hallucinations.

3.1 Background on MLLMs

Consider a sequence $\mathbf{t}^p = [t_1^p, \dots, t_N^p]$ as the input prompt, where t_n^p ($1 \leq n \leq N$) is a prompt token from a predefined vocabulary. Visual tokens $\mathbf{t}^v = [t_1^v, \dots, t_S^v]$ are extracted from visual inputs V . The MLLMs generate the response sequence $\mathbf{y} = [y_1, \dots, y_M]$ using the logit generation function $\mathcal{F}_\theta(\cdot)$ and the softmax function $\sigma(\cdot)$ ¹ as:

$$\mathbf{y} = \sigma(\mathcal{F}_\theta(\mathbf{t}^v, \mathbf{t}^p)). \quad (1)$$

y_m denotes an individual output token for $1 \leq m \leq M$. The conditional probability distribution $p(\mathbf{y}|\mathcal{F}_\theta, \mathbf{t}^p, \mathbf{t}^v)$ can therefore be expressed as:

$$p(\mathbf{y}|\mathcal{F}_\theta, \mathbf{t}^v, \mathbf{t}^p) = \prod_{m=1}^M p(y_m|\mathcal{F}_\theta, \mathbf{t}^v, \mathbf{t}^p, \mathbf{y}_{<m}), \quad (2)$$

where $\mathbf{y}_{<m} = [y_1, \dots, y_{m-1}]$ for $m > 1$ and is empty for $m = 1$. Pre-trained MLLMs encode not only factual knowledge but also statistical correlations and biases from the training data [22, 15]. These biases are encoded within the model parameters (θ^*), enabling self-reflective bias interpretation.

3.2 Gradient-Based Token Influence Estimation

To capture these learned biases, we measure the impact each individual token has on the output logits. To achieve this, we propose token influence estimation based on a first-order Taylor expansion [41] on logit generation function \mathcal{F}_{θ^*} ²:

$$\mathcal{F}_{\theta^*}(\mathbf{t}^v, \mathbf{t}^p)_m \approx \sum_{s=1}^S \mathbf{g}_{ms}^v t_s^v + \sum_{n=1}^N \mathbf{g}_{mn}^p t_n^p + \sum_{i=1}^{m-1} \mathbf{g}_{mi}^y y_i + Const, \quad (3)$$

where

$$\mathbf{g}_{ms}^v := \left. \frac{\partial(\mathcal{F}_{\theta^*})_m}{\partial t_s^v} \right|_{\mathbf{t}^v=\mathbf{t}^{v(0)}}, \quad \mathbf{g}_{mn}^p := \left. \frac{\partial(\mathcal{F}_{\theta^*})_m}{\partial t_n^p} \right|_{\mathbf{t}^p=\mathbf{t}^{p(0)}}, \quad \mathbf{g}_{mi}^y := \left. \frac{\partial(\mathcal{F}_{\theta^*})_m}{\partial y_i} \right|_{\mathbf{y}=\mathbf{y}^{(0)}}, \quad (4)$$

are the first order gradients w.r.t., visual tokens \mathbf{t}^v , text prompt \mathbf{t}^p and previous outputs y_i and $Const$ denotes all other terms that are constant w.r.t., the $\mathbf{t}^v, \mathbf{t}^p$.

We measure the importance of input tokens using the norm of their gradients. Specifically, we use the Manhattan (L1) norm, as it effectively captures the contribution of individual tokens. Accordingly, we represent the influence of each token as $|\mathbf{g}_{m\cdot}^{v/p/y}|$. The overall influence of visual tokens, text prompts, and previous outputs can be represented as:

$$\mathbf{I}_m^v = \sum_{s=1}^S |\mathbf{g}_{ms}^v|, \quad \mathbf{I}_m^p = \sum_{n=1}^N |\mathbf{g}_{mn}^p|, \quad \mathbf{I}_m^y = \sum_{i=1}^{m-1} |\mathbf{g}_{mi}^y|. \quad (5)$$

¹Probability of softmax output is interpreted as confidence.

²Taylor expansion details are in supplementary Sec. A.

This expression allows us to interpret bias at the individual sample level. We also define the influence of each visual token on a specific output vocabulary token c as:

$$I_{ms}(c) = |\mathbf{g}_{ms}^v[c]|, \quad (6)$$

where $\mathbf{g}_{ms}^v[c]$ represents the gradient from the output vocabulary c with respect to the input tokens.

3.3 Influence-Aware Contrastive Decoding

We extend contrastive decoding [28] by incorporating object-aware negative guidance and dynamically computing decoding weights based on token influence. As shown in Fig. 2, for each m^{th} output, contrastive logits are generated alongside the original logits, with the decoding weight α_m inferred based on token influence from both.

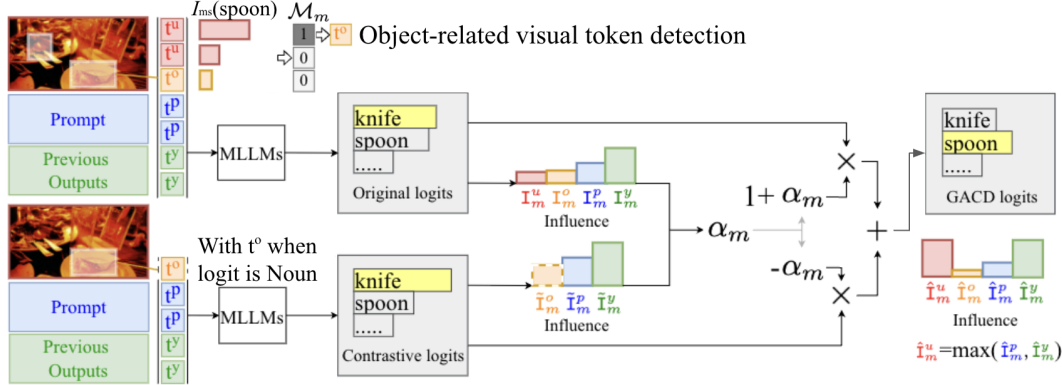


Figure 2: Overview of the proposed GACD method. GACD adjusts contrastive decoding based on token influence (Sec. 3.2), explicitly amplifying the influence of visual tokens \mathbf{t}^u . The contrastive logits, acting as negative guidance, are generated by object-related visual token \mathbf{t}^o , prompt token \mathbf{t}^p , and previous output token \mathbf{t}^y , with object-related visual token \mathbf{t}^o included only for noun predictions to reduce the influence of potential anchor objects and mitigate co-occurrence bias. The decoding weight α_m is calculated based on token influence in both original and contrastive logits, amplifying object-unrelated visual token $\hat{\mathbf{t}}_m^u$ to align with the dominant text component $\max(\hat{\mathbf{t}}_m^p, \hat{\mathbf{t}}_m^y)$. For noun predictions, GACD detects the highest-influence visual token using individual visual influence $I_{ms}(y_m)$ and flags it as object-related \mathbf{t}^o for subsequent processing.

We begin with object-related visual token detection. To identify objects in previous outputs $\mathbf{y}_{<m}$, we first perform noun detection, treating each noun as an object. For each identified object, a mask is applied to flag the highest-influence object-related visual tokens. The mask \mathcal{M}_{ms} fuses visual tokens related to all previously mentioned objects:

$$\mathcal{M}_{ms} := \bigvee_{i=1}^{m-1} \mathcal{M}_{is}, \quad \mathcal{M}_{is} = \begin{cases} 1 & \text{if } s = \arg \max_j I_{ij}(y_i), y_i \text{ is noun} \\ 0 & \text{otherwise} \end{cases}, \quad (7)$$

where \bigvee represents the bitwise OR operator. The visual tokens are categorized into two groups: object-related visual tokens \mathbf{t}^o , and Unrelated Object (UO) tokens \mathbf{t}^u , defined as follows:

$$\mathbf{t}^o = \mathbf{t}^v \odot \mathcal{M}_m, \quad \mathbf{t}^u = \mathbf{t}^v \odot (1 - \mathcal{M}_m), \quad (8)$$

where \odot indicates Hadamard product. The overall influence of these groups is defined as:

$$\mathbf{I}_m^o = \sum_{s=1}^S (|\mathbf{g}_{ms}^v| \odot \mathcal{M}_{ms}), \quad \mathbf{I}_m^u = \sum_{s=1}^S (|\mathbf{g}_{ms}^v| \odot (1 - \mathcal{M}_{ms})), \quad (9)$$

In noun predictions, this mask removes the impact of tokens related to previously mentioned objects \mathbf{t}^o to mitigate co-occurrence bias. For non-noun predictions, this mask calculation is not triggered; all elements in \mathcal{M}_m are set to 0, resulting in an empty \mathbf{t}^o set.

To jointly mitigate text-visual and co-occurrence biases, GACD adjusts the logits as follows:

$$\hat{\mathcal{F}}_{\theta^*}(\mathbf{t}^v, \mathbf{t}^p)_m = (1 + \alpha_m) \mathcal{F}_{\theta^*}(\mathbf{t}^v, \mathbf{t}^p)_m - \alpha_m \mathcal{F}_{\theta^*}(\mathbf{t}^o, \mathbf{t}^p)_m, \quad (10)$$

where α_m is the contrastive decoding weight. This contrastive decoding aims to enlarge the Kullback-Leibler (KL) divergence³ between the contrastive logits distribution $\mathcal{F}_{\theta^*}(\mathbf{t}^o, \mathbf{t}^p)_m$ and the original logits distribution $\mathcal{F}_{\theta^*}(\mathbf{t}^v, \mathbf{t}^p)_m$. Here, the original logits distribution can be viewed as $\mathcal{F}_{\theta^*}(\mathbf{t}^u, \mathbf{t}^o, \mathbf{t}^p)_m$, a joint distribution with additional \mathbf{t}^u . Thus, increasing the KL divergence effectively amplifies the influence of these UO visual tokens \mathbf{t}^u .

The contrastive decoding weight, α_m , controls the KL divergence distance and, from another perspective, regulates the influence of each component on the final GACD logits. The influence of UO visual tokens $\hat{\mathbf{I}}_m^u$, object-related visual tokens $\hat{\mathbf{I}}_m^o$, the prompt $\hat{\mathbf{I}}_m^p$, and previous outputs $\hat{\mathbf{I}}_m^y$ is determined by their gradient values, based on (9) and (5). Follow the chain rule, UO visual tokens are included only in the original logits $\mathcal{F}_{\theta^*}(\mathbf{t}^v, \mathbf{t}^p)_m$ and are amplified by $(1 + \alpha_m)$, while other inputs contribute to the additional contrastive logit $\mathcal{F}_{\theta^*}(\mathbf{t}^o, \mathbf{t}^p)_m$, experiencing smaller gradient changes.

To mitigate text-visual bias, GACD balances the influence of UO visual tokens to align with the dominant text component, defined as $\mathbf{I}_m^t = \max(\mathbf{I}_m^p, \mathbf{I}_m^y)$. Aligning UO visual token influence with the question prompt \mathbf{I}_m^p is crucial for visually grounded responses, while balancing it with previous outputs \mathbf{I}_m^y is essential for preventing visual forgetting. Under this condition, α_m is calculated as:

$$\alpha_m = \frac{\mathbf{I}_m^t - \mathbf{I}_m^v}{\mathbf{I}_m^v - \tilde{\mathbf{I}}_m^o + \tilde{\mathbf{I}}_m^t - \mathbf{I}_m^t}, \tilde{\mathbf{I}}_m^t = \begin{cases} \tilde{\mathbf{I}}_m^p & \text{if } \mathbf{I}_m^p \geq \mathbf{I}_m^y \\ \tilde{\mathbf{I}}_m^y & \text{otherwise} \end{cases} \quad (11)$$

where $\tilde{\mathbf{I}}_m^o$, $\tilde{\mathbf{I}}_m^p$, and $\tilde{\mathbf{I}}_m^y$ represent the influence of object-related visual tokens, prompt, and previous output tokens, respectively, on the contrastive logits $\mathcal{F}_{\theta^*}(\mathbf{t}^o, \mathbf{t}^p)_m$, calculated follow (5).

Furthermore, unlike existing contrastive decoding methods [54, 12, 26], which rely on adaptive plausibility constraints (e.g., prediction confidence) and require experimental tuning to determine optimal thresholds, our method explicitly imposes a constraint to prevent the influence of object-related visual and prompt from becoming negative:

$$\alpha_m = \min(\alpha_m, \frac{\mathbf{I}_m^o}{\tilde{\mathbf{I}}_m^o - \mathbf{I}_m^o}, \frac{\mathbf{I}_m^p}{\tilde{\mathbf{I}}_m^p - \mathbf{I}_m^p}). \quad (12)$$

Additionally, to further mitigate text-visual bias in long-term generation, we propose a sample-dependent stopping criterion based on the visual influence. If the visual influence ratio r_m^v of the token immediately following the end-of-sequence (EOS) token falls below a defined threshold ϵ :

$$r_m^v = \frac{\mathbf{I}_m^v}{\mathbf{I}_m^v + \mathbf{I}_m^p + \mathbf{I}_m^y} < \epsilon \text{ and } y_{m-1} = \text{EOS}, \quad (13)$$

early stopping is triggered to prevent further output generation with minimal visual grounding.

4 Experiments

The proposed method is evaluated for both the open-ended generative tasks and the discriminative tasks. We follow [26, 45, 10, 17] to use Amber [44], MSCOCO [30] and LLaVa-QA90 [32] datasets for the generative task, and Amber [44] and POPE [29] datasets on the discriminative tasks.

Evaluation Metrics. For generative image captioning, we focus on object hallucination and follow [10, 17, 45] report the Caption Hallucination Assessment with Image Relevance (CHAIR) [40] score, which includes sentence-level (hal, C_S) and instance-level (cha, C_I) percentages, instance-level recall (R_{cov}), and the average generated length (Len), as well as co-occurrence object hallucination (cog) and the overall *score* as suggested by [44]. For generative VQA, follow [26, 17] GPT-4V [1] is used to score both accuracy (Acc) and detailedness (Det) on a scale of 10. For discriminative tasks, hallucination manifests as a ‘yes/no’ misclassification we report both accuracy and F1 score.

Implementation Details. The maximum output length is set to 256 across all models, with other model parameters kept at their defaults. To prevent excessive modifications, we set the maximum amplification factor, α_m , to 5 for discriminative tasks and 3 for generative tasks. We empirically set the early stopping thresholds ϵ as follows: LLaVA-v1.5 and LLaVA-v1.6: 7%, InstrucBLIP: 25%, mPLUG-Owl2: 2.5%, and InternVL2: 10%. All experiments are performed on an NVIDIA A40 GPU with batch size of 1. Unless otherwise specified, we use greedy sampling [14].

³A detailed explanation of why contrastive decoding enlarges KL divergence is in supplementary Sec. B.

4.1 Results on Open-ended Generation

In this section, we compare against SOTA alignment-based method RLAIIF-V [48] and contrastive decoding methods VCD [26], M3ID [12], and AVISC [45], on the AMBER and MSCOCO datasets, as presented in Tab. 1, Tab. 2. Additionally, we evaluate our method against VCD on the LLaVA-QA90 dataset, presented in Tab. 3. Our method outperforms most existing approaches across various baseline models and datasets, highlighting its robustness and reliable performance across different data types and model architectures. Specifically, we surpass image-level contrastive decoding methods like VCD and M3ID, demonstrating its effectiveness in operating at the token level and adapting to individual samples. Furthermore, compared to the token-level AVISC, our method excels, likely due to its object awareness and adaptability to fluctuating bias levels. The results further demonstrate that our method effectively mitigates hallucinations while preserving information.

Table 1: Results on the AMBER Dataset.

MLLMs	Method	Generative				Discriminative				Score \uparrow
		cha \downarrow	cov \uparrow	hal \downarrow	cog \downarrow	acc \uparrow	P \uparrow	R \uparrow	F1 \uparrow	
LLaVA v1.5	base	7.8	51.0	36.4	4.2	72.0	93.2	62.4	74.7	83.5
	RLAIIF-V	6.6	49.7	32.0	2.9	76.7	92.0	78.1	84.5	89.0
	VCD	6.7	46.4	32.6	3.5	71.3	91.1	62.3	74.3	83.8
	M3ID	6.2	50.5	29.3	2.8	72.4	91.8	64.1	75.5	84.7
	AVISC	6.5	50.2	34.8	2.7	73.8	89.7	68.4	77.6	85.5
	Ours	5.6	51.0	24.3	1.8	80.3	82.9	89.3	86.0	90.2
Instruct BLIP	base	8.8	52.2	38.2	4.4	76.5	84.5	79.0	81.7	86.5
	RLAIIF-V	7.6	47.7	29.9	2.8	76.5	84.5	79.0	81.7	87.1
	VCD	7.9	49.7	36.7	3.7	75.9	83.5	79.3	81.3	86.7
	M3ID	7.3	49.2	33.8	3.7	75.8	84.4	77.9	81.0	86.9
	AVISC	7.1	48.8	34.4	4.3	75.9	83.4	79.5	81.4	87.2
	Ours	6.0	49.4	26.6	2.4	78.1	88.8	76.6	82.2	88.1
mPLUG Owl2	base	10.6	52.0	39.9	4.5	75.6	95.0	66.9	78.5	84.0
	RLAIIF-V	7.8	50.5	35.7	4.1	81.2	90.8	79.7	84.9	88.6
	VCD	8.0	51.3	35.3	4.1	75.6	83.5	78.8	81.1	86.6
	M3ID	7.8	51.7	34.9	4.1	75.9	83.5	79.3	81.3	86.8
	AVISC	10.9	50.5	35.5	4.4	82.1	90.7	81.4	85.8	87.5
	Ours	7.5	53.6	34.7	4.0	82.1	87.0	86.2	86.6	89.6

Table 2: Results Using the CHAIR Metric on the MSCOCO Subset Following [10].

Method	LLaVA-v1.5				InstructBLIP				mPLUG-Owl2			
	$C_S \downarrow$	$C_I \downarrow$	$R \uparrow$	$Len \uparrow$	$C_S \downarrow$	$C_I \downarrow$	$R \uparrow$	$Len \uparrow$	$C_S \downarrow$	$C_I \downarrow$	$R \uparrow$	$Len \uparrow$
base	48.8	13.4	78.6	99.8	57.8	16.5	73.6	101.3	59.2	17.6	75.8	105.3
VCD	44.8	12.8	76.8	89.8	63.4	19.6	71.2	95.5	52.7	16.1	73.2	93.6
M3ID	44.5	12.1	77.0	85.1	57.3	16.1	72.5	100.1	52.4	15.8	72.7	92.6
AVISC	46.4	13.4	76.3	90.5	58.9	17.8	70.6	99.6	58.3	17.5	75.6	99.5
Ours	41.0	10.9	77.3	85.0	47.4	13.4	72.3	93.9	45.0	12.4	74.9	83.5

Hallucination Mitigation. Our approach achieves hallucination reductions up to 33% at sentence-level (*hal* in Tab. 1 and C_S in Tab. 2) and 32% at instance-level (*cha* in Tab. 1 and C_I in Tab. 2), demonstrating its effectiveness in mitigating overall hallucinations. It also effectively addresses co-occurrence hallucinations, achieving up to a 57% reduction for *cog* in Tab. 1. We detail the text-visual and co-occurrence bias analysis in Sec. 5. Furthermore, an accuracy increase of up to 92% in Tab. 3 underscores our model’s effectiveness in reducing hallucinations by staying closely aligned with the input image. This improvement highlights our method’s capacity to jointly mitigate multiple types of hallucinations.

Information Preservation. Our method also enhances information preservation, with recall (*cov* in Tab. 1 and R in Tab. 2) dropping by an average of only 1.1%, compared to an average drop of 3.2% in other methods, and even increasing by 3.1% when using the baseline mPLUG-Owl2 on the AMBER dataset. Higher recall indicates that our model retrieves a broader range of objects from visual inputs. Additionally, results in Tab. 3 an increase of up to 45% in detailedness (*Det*), further demonstrating our method’s effectiveness in retrieving all relevant visual details and mitigating visual forgetting.

Table 3: Results on LLaVA-QA90 Dataset, with All Settings Following [26].

Method	LLaVA-v1.5		InstructBLIP		mPLUG-Owl2	
	Acc \uparrow	Det \uparrow	Acc \uparrow	Det \uparrow	Acc \uparrow	Det \uparrow
base	3.23	3.54	3.84	4.07	4.07	4.33
VCD	4.15	3.85	4.23	4.69	4.52	4.64
Ours	6.20	5.13	6.28	4.77	6.69	6.28

4.2 Results on Discriminative Task

Next, we evaluate our method on discriminative tasks using AMBER (discriminative VQA) and POPE (existence VQA) datasets, with results shown in Tab. 1 and Tab. 4. The findings confirm that our method achieves a better balance between precision and recall, resulting in consistently higher F1 scores and improved accuracy. Notably, for the high-performance baseline Intern-VL2, other methods degrade its original performance, whereas ours effectively preserves it, likely due to its bias awareness. Additionally, we observe variation in performance improvements across different question categories and baseline MLLMs.

Table 4: Results on POPE in MSCOCO Adversarial Setting.

Method	LLaVA-v1.5		InstructBLIP		mPLUG-Owl2		InternVL2	
	Acc \uparrow	F1 \uparrow	Acc \uparrow	F1 \uparrow	Acc \uparrow	F1 \uparrow	Acc \uparrow	F1 \uparrow
base	79.4	81.6	79.8	81.4	72.5	77.5	85.8	85.0
VCD	80.9	81.3	79.6	79.5	74.2	78.8	83.2	82.2
M3ID	81.7	81.8	81.0	81.6	75.6	79.1	83.5	82.1
AVISC	81.2	81.6	81.8	81.9	80.9	79.7	85.3	84.6
Woodpecker	80.5	80.6	79.0	78.6	77.5	76.9	85.7	84.8
Ours	83.5	82.1	82.5	82.1	84.2	83.7	85.8	85.0

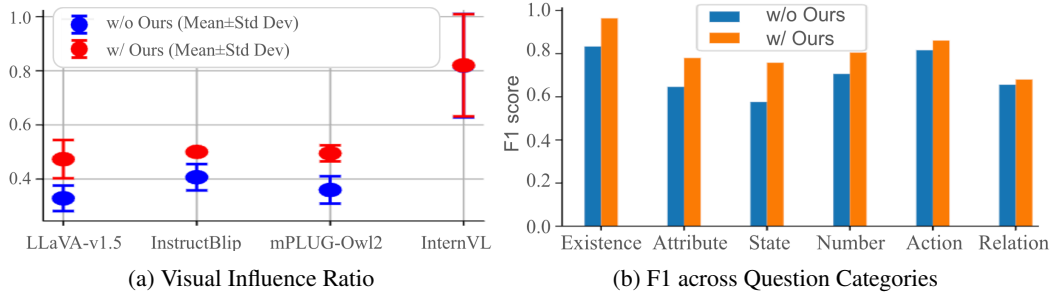


Figure 3: (a) Visual influence ratios across the POPE dataset, illustrating variation across MLLMs. Our method successfully increases the visual influence ratio when it falls below 50%. (b) F1 scores for the AMBER discriminative task using LLaVA-v1.5 are consistently improved by our method, with particularly notable gains in the existence and state categories.

Variation in Improvement Across Question Categories. Fig. 3b presents F1 scores across various question categories using baseline model LLaVA-v1.5 [31]. Our method improves performance across all categories, with particularly significant gains in existence, attributes, and state. These improvements can be attributed to the enhanced influence of visual tokens, which benefit categories that are more readily discernible from visual inputs.

Variation in Improvement Across MLLMs. Our method achieves the most significant improvement on mPLUG-Owl2 in object existence VQA (Tab. 4) and on LLaVA-v1.5 across various VQA categories (Tab. 1 discriminative), with minor improvement observed on InternVL2. This variation in performance correlates with the baseline visual influence ratios of the MLLMs. Fig. 3a presents the visual influence ratios in object existence VQA, showing that LLaVA-v1.5 exhibits the lowest visual contribution, followed by mPLUG-Owl2. This lower baseline visual influence ratio allows our method to make more impactful adjustments. In contrast, InternVL2 has an original visual influence ratio exceeding 50%, resulting in minimal improvement when our method is applied. The strong performance of InternVL2 can be attributed to its original high visual influence ratio, further validating the motivation behind our approach. However, this dominant visual influence ratio in

InternVL2 is not consistent across other question categories or in open-ended generation tasks ⁴, which allows our method to enhance its performance on the AMBER dataset (Tab. 6).

4.3 Results on Additional MLLMs and Datasets

We further evaluate modern MLLMs, LLaVA-v1.6 and Intern-VL2, on the Amber dataset. The results in Tab. 6 in supplementary demonstrate that our method consistently improves MLLM performance, even when their original performance is high. To further evaluate the effectiveness of our method across diverse tasks, we conduct evaluations on the MMBench [33] and MMVet [49] datasets. The results are presented in supplementary Tab. 8 and Tab. 9. The evaluation results show that our method enhances perception and recognition performance, particularly in tasks where visual contribution is straightforward. Moreover, it maintains overall task performance, demonstrating its robustness.

5 Ablation Study

In this section, we first analyze text–visual and co-occurrence biases, and then study the contributions of our proposed components. Further details on gradient computation methods, norm selection, and hyperparameter settings are provided in the supplementary material.

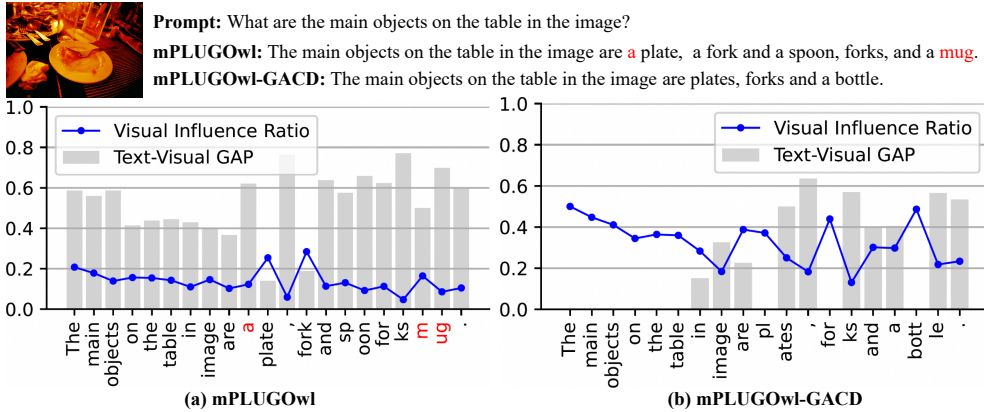


Figure 4: Comparison of visual influence ratios r_m^v and Text-Visual GAP, with and without our GACD. (a) Without GACD, the baseline mPLUG-Owl2 shows a low initial visual influence, while objects in images initially have relatively high visual influence, which decreases as sequence length grows. Hallucinations tend to occur when the visual ratio is low. The text-visual gap confirms that text dominates the influence on predictions. (b) With GACD, the visual influence ratio increases overall and mitigates the decrease over the sequence length. The text tokens only domain influence in predictions less related to the visual, reducing hallucination.

Text-Visual Bias Analysis. Fig. 3a shows that with the exception of InternVL2, MLLMs – LLaVA-v1.5, InstructBLIP, and mPLUG-Owl2 – rely more on text prompt than on visual input. Likely due to MLLMs’ training process, this tendency is common in MLLMs, where multimodal features are aligned with language tokens after extensive text-based pre-training, causing language components to dominate decision-making. GACD effectively increases overall visual influence to match that of object-present question prompts in POPE (Fig. 3a). In the open-ended generation task, we further observe the visual influence ratio r_m^v and the Text-Visual GAP, defined as $\max(\max(r_m^p, r_m^y) - r_m^v, 0)$, the difference between the text influence ratio and the visual influence ratio when text influence is dominant ⁵. Observations in Fig. 4 also highlight the text-dominant influence typical of MLLMs. GACD counteracts this by boosting the influence of visual tokens when aligning them with prompts and previous outputs, leading to higher prediction confidence and a reduction in hallucinations (see Fig. 6 in supplementary). Additionally, the nature of the output token affects the degree of visual influence ratio. For instance, punctuation marks or suffixes tend to have a lower visual influence ratio. This is intuitive, as these tokens rely more on linguistic context and are less dependent

⁴Results for other question categories and visualizations of open-ended generation are in supplementary Tab. 20 and Fig. 9.

⁵ r_m^p and r_m^y are derived in the same manner as r_m^v in (13).

on visual information. This observation highlights the value of our GACD framework delivering sample-dependent, token-specific hallucination mitigation.

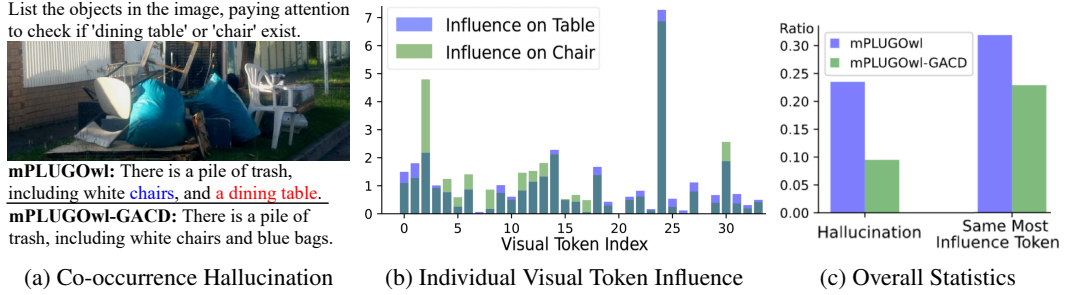


Figure 5: Co-occurrence hallucination of ‘table’ in the presence of ‘chair’. (a) Comparison of outputs with and without GACD. (b) Visualization of individual visual token influence indicates that the visual token with index 24, which has the highest influence on the hallucinated ‘table’, also holds the highest influence on ‘chair’. (c) Summary statistics for 100 chair-only and 100 table-only images, showing the hallucination rate and the percentage of cases where both objects share the same most influential visual token (as illustrated in b). GACD effectively reduces both metrics.

Co-occurrence Bias Analysis. Fig. 5a shows an example where mPLUG-Owl2 incorrectly predicts ‘dining table’ due to the presence of a ‘chair’ in the image. In Fig. 5b, the influence of individual visual tokens on hallucinated prediction I_{ms} (‘table’) and I_{ms} (‘chair’) shows that they share the same most influential visual token: $s = 24$. We further collected 100 chair-only and 100 table-only images from MSCOCO evaluation dataset [30]. Experimental results in Fig. 5c indicate that when either only ‘chair’ or ‘table’ exists in the image, the hallucination rate for the other object is 23.5%, with a shared most influential visual token rate of 31.9% in these hallucinations. This indicates that the ‘Same Most Influential Token’ phenomenon is common in co-occurrence hallucinations. Our GACD effectively reduces the hallucination where both ‘table’ or ‘chair’ are predicted in single-object images.

5.1 Component Analysis

To assess the effectiveness of each component in our proposed method, we conducted the following analyses: 1) Visual Amplification (VA) only: Applied visual amplification to all visual tokens, including during noun predictions. 2) Co-occurrence Hallucination Reduction (CR): Detected object-related visual tokens and amplified UO visual tokens during noun predictions. 3) Our full model, with early stopping (ES). Tab. 5 demonstrates that each component of our method contributes to the overall performance. VA significantly reduces hallucinations while improving object recall. CR further mitigates co-occurrence bias, a residual form of the text-visual bias addressed by VA, resulting in additional hallucination reduction. When needed, ES mechanism shortens output length to effectively reduce hallucinations with only a minor trade-off in object recall.

Table 5: Component Analysis Using the CHAIR Metric.

Components			LLaVA-v1.5				InstructBLIP				mPLUG-Owl2			
VA	CR	ES	$C_S \downarrow$	$C_I \downarrow$	$R \uparrow$	$Len \uparrow$	$C_S \downarrow$	$C_I \downarrow$	$R \uparrow$	$Len \uparrow$	$C_S \downarrow$	$C_I \downarrow$	$R \uparrow$	$Len \uparrow$
			48.8	13.4	78.6	99.8	57.8	16.5	73.6	101.3	59.2	17.6	75.8	105.3
✓			46.4	11.6	79.0	95.6	53.6	15.1	75.3	108.4	52.6	14.4	78.2	95.6
✓	✓		46.2	11.3	79.4	95.5	53.2	14.0	74.6	105.7	52.3	14.2	78.0	95.5
✓	✓	✓	41.0	10.9	77.3	85.0	47.4	13.4	72.3	93.9	45.0	12.4	74.9	83.5

6 Conclusion

In conclusion, we introduce a gradient-based self-reflection method to estimate token influence and quantitatively estimate bias severity. This estimation enables the identification of object-related visual tokens, which are then integrated into an influence-aware contrastive decoding framework. This framework effectively mitigates both text-visual and co-occurrence biases, reducing hallucinations. Our method operates without requiring additional resources such as costly fine-tuning, extra models, or data statistics. Furthermore, to reduce text-visual bias in long-generated sequences, we propose a sample-dependent stopping criterion based on the proposed visual influence.

References

- [1] Josh Achiam, Steven Adler, Sandhini Agarwal, Lama Ahmad, Ilge Akkaya, Florencia Leoni Aleman, Diogo Almeida, Janko Altschmidt, Sam Altman, Shyamal Anadkat, et al. Gpt-4 technical report. *arXiv preprint arXiv:2303.08774*, 2023.
- [2] Jinze Bai, Shuai Bai, Shusheng Yang, Shijie Wang, Sinan Tan, Peng Wang, Junyang Lin, Chang Zhou, and Jingren Zhou. Qwen-vl: A frontier large vision-language model with versatile abilities. *arXiv preprint arXiv:2308.12966*, 2023.
- [3] Assaf Ben-Kish, Moran Yanuka, Morris Alper, Raja Giryes, and Hadar Averbuch-Elor. Mocha: Multi-objective reinforcement mitigating caption hallucinations. *arXiv preprint arXiv:2312.03631*, 2023.
- [4] Jun Chen, Deyao Zhu, Xiaoqian Shen, Xiang Li, Zechun Liu, Pengchuan Zhang, Raghuraman Krishnamoorthi, Vikas Chandra, Yunyang Xiong, and Mohamed Elhoseiny. Minigpt-v2: large language model as a unified interface for vision-language multi-task learning. *arXiv preprint arXiv:2310.09478*, 2023.
- [5] Zhaorun Chen, Zhuokai Zhao, Hongyin Luo, Huaxiu Yao, Bo Li, and Jiawei Zhou. Halc: Object hallucination reduction via adaptive focal-contrast decoding. *arXiv preprint arXiv:2403.00425*, 2024.
- [6] Zhe Chen, Jiannan Wu, Wenhai Wang, Weijie Su, Guo Chen, Sen Xing, Muyan Zhong, Qinglong Zhang, Xizhou Zhu, Lewei Lu, et al. Internvl: Scaling up vision foundation models and aligning for generic visual-linguistic tasks. In *Proceedings of the IEEE/CVF Conference on Computer Vision and Pattern Recognition*, pages 24185–24198, 2024.
- [7] Zhiyang Chen, Yousong Zhu, Yufei Zhan, Zhaowen Li, Chaoyang Zhao, Jinqiao Wang, and Ming Tang. Mitigating hallucination in visual language models with visual supervision. *arXiv preprint arXiv:2311.16479*, 2023.
- [8] Yung-Sung Chuang, Yujia Xie, Hongyin Luo, Yoon Kim, James Glass, and Pengcheng He. Dola: Decoding by contrasting layers improves factuality in large language models. *arXiv preprint arXiv:2309.03883*, 2023.
- [9] Wenliang Dai, Junnan Li, Dongxu Li, Anthony Meng Huat Tiong, Junqi Zhao, Weisheng Wang, Boyang Li, Pascale Fung, and Steven Hoi. Instructblip: Towards general-purpose vision-language models with instruction tuning, 2023.
- [10] Ailin Deng, Zhirui Chen, and Bryan Hooi. Seeing is believing: Mitigating hallucination in large vision-language models via clip-guided decoding. *arXiv preprint arXiv:2402.15300*, 2024.
- [11] Joseph Enguehard. Sequential integrated gradients: a simple but effective method for explaining language models. *arXiv preprint arXiv:2305.15853*, 2023.
- [12] Alessandro Favero, Luca Zancato, Matthew Trager, Siddharth Choudhary, Pramuditha Perera, Alessandro Achille, Ashwin Swaminathan, and Stefano Soatto. Multi-modal hallucination control by visual information grounding. *arXiv preprint arXiv:2403.14003*, 2024.
- [13] Chaoyou Fu, Peixian Chen, Yunhang Shen, Yulei Qin, Mengdan Zhang, Xu Lin, Jinrui Yang, Xiawu Zheng, Ke Li, Xing Sun, Yunsheng Wu, and Rongrong Ji. Mme: A comprehensive evaluation benchmark for multimodal large language models, 2024.
- [14] Alex Graves. Generating sequences with recurrent neural networks. *arXiv preprint arXiv:1308.0850*, 2013.
- [15] Yufei Guo, Muzhe Guo, Juntao Su, Zhou Yang, Mengqiu Zhu, Hongfei Li, Mengyang Qiu, and Shuo Shuo Liu. Bias in large language models: Origin, evaluation, and mitigation. *arXiv preprint arXiv:2411.10915*, 2024.
- [16] Lei Huang, Weijiang Yu, Weitao Ma, Weihong Zhong, Zhangyin Feng, Haotian Wang, Qianglong Chen, Weihua Peng, Xiaocheng Feng, Bing Qin, et al. A survey on hallucination in large language models: Principles, taxonomy, challenges, and open questions. *ACM Transactions on Information Systems*, 43(2):1–55, 2025.

- [17] Qidong Huang, Xiaoyi Dong, Pan Zhang, Bin Wang, Conghui He, Jiaqi Wang, Dahua Lin, Weiming Zhang, and Nenghai Yu. Opera: Alleviating hallucination in multi-modal large language models via over-trust penalty and retrospection-allocation. In *Proceedings of the IEEE/CVF Conference on Computer Vision and Pattern Recognition*, pages 13418–13427, 2024.
- [18] Chaoya Jiang, Haiyang Xu, Mengfan Dong, Jiaying Chen, Wei Ye, Ming Yan, Qinghao Ye, Ji Zhang, Fei Huang, and Shikun Zhang. Hallucination augmented contrastive learning for multimodal large language model. In *Proceedings of the IEEE/CVF Conference on Computer Vision and Pattern Recognition*, pages 27036–27046, 2024.
- [19] Zhehan Kan, Ce Zhang, Zihan Liao, Yapeng Tian, Wenming Yang, Junyuan Xiao, Xu Li, Dongmei Jiang, Yaowei Wang, and Qingmin Liao. Catch: Complementary adaptive token-level contrastive decoding to mitigate hallucinations in llms, 2024.
- [20] Cheongwoong Kang and Jaesik Choi. Impact of co-occurrence on factual knowledge of large language models. *arXiv preprint arXiv:2310.08256*, 2023.
- [21] Andrei Kapishnikov, Subhashini Venugopalan, Besim Avci, Ben Wedin, Michael Terry, and Tolga Bolukbasi. Guided integrated gradients: An adaptive path method for removing noise. In *Proceedings of the IEEE/CVF conference on computer vision and pattern recognition*, pages 5050–5058, 2021.
- [22] Byungju Kim, Hyunwoo Kim, Kyungsu Kim, Sungjin Kim, and Junmo Kim. Learning not to learn: Training deep neural networks with biased data. In *Proceedings of the IEEE/CVF conference on computer vision and pattern recognition*, pages 9012–9020, 2019.
- [23] Younghyun Kim, Sangwoo Mo, Minkyu Kim, Kyungmin Lee, Jaeho Lee, and Jinwoo Shin. Discovering and mitigating visual biases through keyword explanation. In *Proceedings of the IEEE/CVF Conference on Computer Vision and Pattern Recognition*, pages 11082–11092, 2024.
- [24] Katherine Lee, Daphne Ippolito, Andrew Nystrom, Chiyuan Zhang, Douglas Eck, Chris Callison-Burch, and Nicholas Carlini. Deduplicating training data makes language models better. In Smaranda Muresan, Preslav Nakov, and Aline Villavicencio, editors, *Proceedings of the 60th Annual Meeting of the Association for Computational Linguistics (Volume 1: Long Papers)*, pages 8424–8445, Dublin, Ireland, May 2022. Association for Computational Linguistics.
- [25] Nayeon Lee, Wei Ping, Peng Xu, Mostofa Patwary, Pascale N Fung, Mohammad Shoeybi, and Bryan Catanzaro. Factuality enhanced language models for open-ended text generation. *Advances in Neural Information Processing Systems*, 35:34586–34599, 2022.
- [26] Sicong Leng, Hang Zhang, Guanzheng Chen, Xin Li, Shijian Lu, Chunyan Miao, and Lidong Bing. Mitigating object hallucinations in large vision-language models through visual contrastive decoding. In *Proceedings of the IEEE/CVF Conference on Computer Vision and Pattern Recognition*, pages 13872–13882, 2024.
- [27] Kenneth Li, Oam Patel, Fernanda Viégas, Hanspeter Pfister, and Martin Wattenberg. Inference-time intervention: Eliciting truthful answers from a language model. *Advances in Neural Information Processing Systems*, 36:41451–41530, 2023.
- [28] Xiang Lisa Li, Ari Holtzman, Daniel Fried, Percy Liang, Jason Eisner, Tatsunori Hashimoto, Luke Zettlemoyer, and Mike Lewis. Contrastive decoding: Open-ended text generation as optimization. *arXiv preprint arXiv:2210.15097*, 2022.
- [29] Yifan Li, Yifan Du, Kun Zhou, Jinpeng Wang, Wayne Xin Zhao, and Ji-Rong Wen. Evaluating object hallucination in large vision-language models. *arXiv preprint arXiv:2305.10355*, 2023.
- [30] Tsung-Yi Lin, Michael Maire, Serge Belongie, James Hays, Pietro Perona, Deva Ramanan, Piotr Dollár, and C Lawrence Zitnick. Microsoft coco: Common objects in context. In *Computer Vision—ECCV 2014: 13th European Conference, Zurich, Switzerland, September 6–12, 2014, Proceedings, Part V 13*, pages 740–755. Springer, 2014.
- [31] Haotian Liu, Chunyuan Li, Yuheng Li, Bo Li, Yuanhan Zhang, Sheng Shen, and Yong Jae Lee. Llava-next: Improved reasoning, ocr, and world knowledge, 2024.

- [32] Haotian Liu, Chunyuan Li, Qingyang Wu, and Yong Jae Lee. Visual instruction tuning. *Advances in neural information processing systems*, 36, 2024.
- [33] Yuan Liu, Haodong Duan, Yuanhan Zhang, Bo Li, Songyang Zhang, Wangbo Zhao, Yike Yuan, Jiaqi Wang, Conghui He, Ziwei Liu, et al. Mmbench: Is your multi-modal model an all-around player? In *European Conference on Computer Vision*, pages 216–233. Springer, 2025.
- [34] Daniel D Lundstrom, Tianjian Huang, and Meisam Razaviyayn. A rigorous study of integrated gradients method and extensions to internal neuron attributions. In *International Conference on Machine Learning*, pages 14485–14508. PMLR, 2022.
- [35] Avshalom Manevich and Reut Tsarfaty. Mitigating hallucinations in large vision-language models (lvllms) via language-contrastive decoding (lcd), 2024.
- [36] Ariana Martino, Michael Iannelli, and Coleen Truong. Knowledge injection to counter large language model (llm) hallucination. In *European Semantic Web Conference*, pages 182–185. Springer, 2023.
- [37] Nick McKenna, Tianyi Li, Liang Cheng, Mohammad Javad Hosseini, Mark Johnson, and Mark Steedman. Sources of hallucination by large language models on inference tasks. *arXiv preprint arXiv:2305.14552*, 2023.
- [38] Yeji Park, Deokyeong Lee, Junsuk Choe, and Buru Chang. Convis: Contrastive decoding with hallucination visualization for mitigating hallucinations in multimodal large language models. *arXiv preprint arXiv:2408.13906*, 2024.
- [39] Alec Radford, Jong Wook Kim, Chris Hallacy, Aditya Ramesh, Gabriel Goh, Sandhini Agarwal, Girish Sastry, Amanda Askell, Pamela Mishkin, Jack Clark, et al. Learning transferable visual models from natural language supervision. In *International conference on machine learning*, pages 8748–8763. PMLR, 2021.
- [40] Anna Rohrbach, Lisa Anne Hendricks, Kaylee Burns, Trevor Darrell, and Kate Saenko. Object hallucination in image captioning. *arXiv preprint arXiv:1809.02156*, 2018.
- [41] Michael Spivak. *Calculus*. houston, tx: Publish or perish, 1980.
- [42] Zhiqing Sun, Sheng Shen, Shengcao Cao, Haotian Liu, Chunyuan Li, Yikang Shen, Chuang Gan, Liang-Yan Gui, Yu-Xiong Wang, Yiming Yang, et al. Aligning large multimodal models with factually augmented rlhf. *arXiv preprint arXiv:2309.14525*, 2023.
- [43] SM Tonmoy, SM Zaman, Vinija Jain, Anku Rani, Vipula Rawte, Aman Chadha, and Amitava Das. A comprehensive survey of hallucination mitigation techniques in large language models. *arXiv preprint arXiv:2401.01313*, 2024.
- [44] Junyang Wang, Yuhang Wang, Guohai Xu, Jing Zhang, Yukai Gu, Haitao Jia, Ming Yan, Ji Zhang, and Jitao Sang. An llm-free multi-dimensional benchmark for mllms hallucination evaluation. *arXiv preprint arXiv:2311.07397*, 2023.
- [45] Sangmin Woo, Donguk Kim, Jaehyuk Jang, Yubin Choi, and Changick Kim. Don’t miss the forest for the trees: Attentional vision calibration for large vision language models. *arXiv preprint arXiv:2405.17820*, 2024.
- [46] Shangyu Xing, Fei Zhao, Zhen Wu, Tuo An, Weihao Chen, Chunhui Li, Jianbing Zhang, and Xinyu Dai. Efuf: Efficient fine-grained unlearning framework for mitigating hallucinations in multimodal large language models. *arXiv preprint arXiv:2402.09801*, 2024.
- [47] Qinghao Ye, Haiyang Xu, Jiabo Ye, Ming Yan, Anwen Hu, Haowei Liu, Qi Qian, Ji Zhang, and Fei Huang. mplug-owl2: Revolutionizing multi-modal large language model with modality collaboration. In *Proceedings of the IEEE/CVF Conference on Computer Vision and Pattern Recognition*, pages 13040–13051, 2024.
- [48] Tianyu Yu, Haoye Zhang, Yuan Yao, Yunkai Dang, Da Chen, Xiaoman Lu, Ganqu Cui, Taiwen He, Zhiyuan Liu, Tat-Seng Chua, et al. Rlaif-v: Aligning mllms through open-source ai feedback for super gpt-4v trustworthiness. *arXiv preprint arXiv:2405.17220*, 2024.

- [49] Weihao Yu, Zhengyuan Yang, Linjie Li, Jianfeng Wang, Kevin Lin, Zicheng Liu, Xinchao Wang, and Lijuan Wang. Mm-vet: Evaluating large multimodal models for integrated capabilities. *arXiv preprint arXiv:2308.02490*, 2023.
- [50] Zihao Yue, Liang Zhang, and Qin Jin. Less is more: Mitigating multimodal hallucination from an eos decision perspective. *arXiv preprint arXiv:2402.14545*, 2024.
- [51] Bohan Zhai, Shijia Yang, Chenfeng Xu, Sheng Shen, Kurt Keutzer, Chunyuan Li, and Manling Li. Halle-control: Controlling object hallucination in large multimodal models, 2024.
- [52] Yi-Fan Zhang, Weichen Yu, Qingsong Wen, Xue Wang, Zhang Zhang, Liang Wang, Rong Jin, and Tieniu Tan. Debiasing large visual language models. *arXiv preprint arXiv:2403.05262*, 2024.
- [53] Linxi Zhao, Yihe Deng, Weitong Zhang, and Quanquan Gu. Mitigating object hallucination in large vision-language models via classifier-free guidance. *arXiv preprint arXiv:2402.08680*, 2024.
- [54] Yiyang Zhou, Chenhang Cui, Jaehong Yoon, Linjun Zhang, Zhun Deng, Chelsea Finn, Mohit Bansal, and Huaxiu Yao. Analyzing and mitigating object hallucination in large vision-language models. *arXiv preprint arXiv:2310.00754*, 2023.

A First Order Taylor Expansion

The first order Taylor expansion of \mathcal{F}_{θ^*} w.r.t., $\mathbf{t}^v, \mathbf{t}^p$ and, all the previous output tokens \mathbf{y}_i with $i < m$:

$$\begin{aligned}\mathcal{F}_{\theta^*}(\mathbf{t}^v, \mathbf{t}^p)_m &\approx \mathcal{F}_{\theta^*}(\mathbf{t}^{v(0)}, \mathbf{t}^{p(0)})_m + \sum_{s=1}^S \frac{\partial(\mathcal{F}_{\theta^*})_m}{\partial t_s^v} \Big|_{\mathbf{t}^{v(0)}} (t_s^v - t_s^{v(0)}) \\ &\quad + \sum_{n=1}^N \frac{\partial(\mathcal{F}_{\theta^*})_m}{\partial t_n^p} \Big|_{\mathbf{t}^{p(0)}} (t_n^p - t_n^{p(0)}) + \sum_{i=1}^{m-1} \frac{\partial(\mathcal{F}_{\theta^*})_m}{\partial y_i} \Big|_{\mathbf{y}_i^{(0)}} (y_i - y_i^{(0)}) \quad (14) \\ &= \sum_{s=1}^S \mathbf{g}_{ms}^v t_s^v + \sum_{n=1}^N \mathbf{g}_{mn}^p t_n^p + \sum_{i=1}^{m-1} \mathbf{g}_{mi}^y y_i + Const,\end{aligned}$$

where $\mathbf{g}_{ms}^v = \frac{\partial(\mathcal{F}_{\theta^*})_m}{\partial t_s^v} \Big|_{\mathbf{t}^v=\mathbf{t}^{v(0)}}$, $\mathbf{g}_{mn}^p = \frac{\partial(\mathcal{F}_{\theta^*})_m}{\partial t_n^p} \Big|_{\mathbf{t}^p=\mathbf{t}^{p(0)}}$ and $\mathbf{g}_{mi}^y = \frac{\partial(\mathcal{F}_{\theta^*})_m}{\partial y_i} \Big|_{\mathbf{y}_i=\mathcal{F}_{\theta^*}(\mathbf{t}^{v(0)}, \mathbf{t}^{p(0)})}$ are the first order gradients w.r.t., visual tokens \mathbf{t}^v , text prompt \mathbf{t}^p and previous outputs y_i and $Const$ denotes all other terms that are constant w.r.t., the $\mathbf{t}^v, \mathbf{t}^p$.

B Interpreting Contrastive Decoding through KL Divergence

Kullback-Leibler (KL) divergence can be used to interpret contrastive decoding, For example, in GACD VA mode, it measures the divergence between the reference distribution $p(y_{cm}|\mathcal{F}_{\theta^*}, \mathbf{t}^v, y_{<m})$ to the visual joint distribution $p(y_{cm}|\mathcal{F}_{\theta^*}, \mathbf{t}^v, \mathbf{t}^p, y_{<m})$.

$$\begin{aligned}D_{KL} &= \sum_c p(y_{cm}|\mathcal{F}_{\theta^*}, \mathbf{t}^v, \mathbf{t}^p, y_{<m}) \log\left(\frac{p(y_{cm}|\mathcal{F}_{\theta^*}, \mathbf{t}^v, \mathbf{t}^p, y_{<m})}{p(y_{cm}|\mathcal{F}_{\theta^*}, \mathbf{t}^p, y_{<m})}\right) \\ &= \sum_c p(y_{cm}|\mathcal{F}_{\theta^*}, \mathbf{t}^v, \mathbf{t}^p, y_{<m}) (\log(p(y_{cm}|\mathcal{F}_{\theta^*}, \mathbf{t}^v, \mathbf{t}^p, y_{<m})) - \log(p(y_{cm}|\mathcal{F}_{\theta^*}, \mathbf{t}^p, y_{<m}))) \\ &= \sum_c p(y_{cm}|\mathcal{F}_{\theta^*}, \mathbf{t}^v, \mathbf{t}^p, y_{<m}) (\mathcal{F}_{\theta^*}(\mathbf{t}^v, \mathbf{t}^p)_m[c] - \log(\sum \exp(\mathcal{F}_{\theta^*}(\mathbf{t}^v, \mathbf{t}^p)_m)) \\ &\quad - \mathcal{F}_{\theta^*}(\mathbf{t}^p)_m[c] + \log(\sum \exp(\mathcal{F}_{\theta^*}(\mathbf{t}^p)_m))) \\ &= \sum_c p(y_{cm}|\mathcal{F}_{\theta^*}, \mathbf{t}^v, \mathbf{t}^p, y_{<m}) (\underbrace{(\mathcal{F}_{\theta^*}(\mathbf{t}^v, \mathbf{t}^p)_m - \mathcal{F}_{\theta^*}(\mathbf{t}^p)_m)[c]}_{\text{adjustment term}} + Const), \quad (15)\end{aligned}$$

where $p(y_{cm}|\mathcal{F}_{\theta^*}, \mathbf{t}^v, \mathbf{t}^p, y_{<m}) = \sigma(\mathcal{F}_{\theta^*}(\mathbf{t}^v, \mathbf{t}^p)_m)$, $p(y_{cm}|\mathcal{F}_{\theta^*}, \mathbf{t}^p, y_{<m}) = \sigma(\mathcal{F}_{\theta^*}(\mathbf{t}^p)_m)$ and c represents a class in the predefined vocabulary. The adjustment term $\mathcal{F}_{\theta^*}(\mathbf{t}^v, \mathbf{t}^p)_m - \mathcal{F}_{\theta^*}(\mathbf{t}^p)_m$ increases the KL divergence, thereby emphasizing the impact of visual tokens.

C Result on modern MLLMs

We further evaluate modern MLLMs, LLaVA-v1.6 and Intern-VL2, on the Amber dataset. The results in Tab. 6 demonstrate that our method consistently improves MLLM performance, even when their original performance is high.

Table 6: Latest MLLMs on the AMBER Dataset.

MLLMs	Method	Generative				Discriminative				Score \uparrow
		cha \downarrow	cov \uparrow	hal \downarrow	cog \downarrow	acc \uparrow	P \uparrow	R \uparrow	F1 \uparrow	
LLaVA v1.6	base	9.9	56.7	47.4	4.3	80.3	82.9	89.3	86.0	88.5
	Ours	8.7	58.3	43.8	2.5	81.2	85.2	88.8	87.0	89.2
Intern VL2	base	8.1	69.6	59.0	5.2	84.0	87.3	88.8	88.0	90.0
	Ours	7.9	69.8	57.8	3.7	84.7	88.2	88.8	88.5	90.3

D MLLMs Architectures

Tab. 7 shows detailed information about the vision encoder and LLM components of the MLLM architectures used in our experiments.

Table 7: Details of the used MLLM architectures.

MLLMs	Vision encoder	LLM
LLaVA-v1.5 (7B)	CLIP-L-336px	Vicuna-v1.5-7B
LLaVA-v1.5-13B	CLIP-L-336px	Vicuna-v1.5-13B
LLaVA-v1.6	CLIP-L-336px	Vicuna-v1.5-7B
InstructBLIP (7B)	BLIP-2	Vicuna-v1.1-7B
InstructBLIP-13B	BLIP-2	Vicuna-v1.1-13B
mPLUG-Owl2	CLIP-L	LLaMA-2-7B
InternVL2-4B	InternViT-300M-448px	Phi-3-mini-128k-instruct

E Results on MMBench

We further evaluate our method on MMBench [33]. The results in Tab. 8 indicate that our method improves the overall performance and achieves consistent improvements across MLLMs on Coarse Perception (CP). This outcome aligns with the intended effect of our method, as its focus on increasing visual influence is directly linked to improving coarse perception capabilities. For other metrics, our method yields minor improvements due to the possible reason that certain abilities, such as Logical Reasoning (LR), rely more on the language component of MLLMs and cannot be enhanced solely by increasing visual influence.

Table 8: Results on MMBench Dataset.

MLLMs	Method	Overall	CP	FP-S	FP-C	AR	LR	RR
LLaVA-V1.5	base	62.3	68.5	69.6	57.7	73.1	29.9	54.7
	ours	61.8	73.2	62.6	53.0	73.3	27.8	57.8
mPLUG-Owl2	base	63.5	68.1	69.1	55.8	78.4	37.0	57.0
	ours	65.0	72.6	66.6	53.0	76.0	41.6	63.0

F Results on MM-Vet

The evaluation on MM-Vet [49] in Tab. 9 shows that our method achieves consistent overall (Total) improvement, along with enhancements in recognition (Rec) and Optical Character Recognition (OCR), indicating its effectiveness in improving visual recognition. However, its performance varies across other metrics, including knowledge (Know), generalization (Gen), spatial awareness (Spat), and math (Math), suggesting that our method, which focuses on token influence balancing, may not effectively enhance the generalization ability of MLLMs.

Table 9: Results on MM-Vet dataset.

MLLMs	Method	Rec	OCR	Know	Gen	Spat	Math	Total
LLaVA-V1.5	base	32.9	20.1	19.0	20.1	25.6	5.2	28.0
	ours	38.9	24.9	15.0	15.5	24.9	7.7	28.9
InstructBlip	base	32.4	14.6	16.5	18.2	18.6	7.7	26.2
	ours	40.5	18.0	18.7	17.4	14.9	3.8	26.6
mPLUG-Owl2	base	36.1	19.4	29.8	19.4	23.9	7.7	27.3
	ours	45.0	26.4	27.9	25.9	24.8	3.8	33.9

G Results on MME

Our evaluation on MME [13] dataset is presented in Tab. 10. Our method achieves better overall (Total) results and equal or improved performance in existence and counting, demonstrating its

effectiveness in object recognition. However, it does not improve position accuracy and exhibits varying behavior on color. This diversity may stem from the inherent capabilities of MLLMs, which cannot be solely enhanced through token influence balancing.

Table 10: Result on MME Dataset.

MLLMs	Method	Existence \uparrow	Count \uparrow	Position \uparrow	Color \uparrow	Total \uparrow
LLaVA-v1.5	base	190.0	140.0	128.3	155.0	613.3
	ours	190.0	153.3	128.3	163.3	634.9
InstructBLIP	base	180.0	55.0	50.0	130.0	415.0
	ours	185.0	55.0	50.0	130.0	420.0
mPLUG-Owl2	base	170.0	145.0	73.3	158.3	546.6
	ours	170.0	150.0	73.3	150.0	548.3

H Other Results of POPE

We report our experimental results on the POPE dataset, in addition to MSCOCO and adversarial settings, in Tab. 11. The results indicate that our method improves performance across all baseline MLLMs, with more significant gains observed in the adversarial setting. This discrepancy likely arises because adversarial scenarios require models to rely more heavily on visual inputs, aligning with our method’s focus on enhancing visual influence. Conversely, for popular and random objects, textual data often provides sufficient statistical information, reducing the necessity for increased visual input reliance.

Table 11: More Results on POPE [29].

Dataset	Setting	Method	LLaVA-v1.5		InstructBLIP		mPLUG-Owl2	
			Acc \uparrow	F1 \uparrow	Acc \uparrow	F1 \uparrow	Acc \uparrow	F1 \uparrow
MSCOCO	Random	base	86.5	84.8	87.1	85.7	86.0	84.4
		ours	86.8	85.1	87.9	86.8	87.9	87.1
	Popular	base	85.5	83.8	84.2	83.6	84.6	83.2
		ours	85.6	84.0	85.0	84.3	86.4	85.7
A-OKVQA	Random	base	88.0	87.6	88.5	88.5	86.5	85.7
		ours	88.1	87.4	88.8	88.8	88.4	88.1
	Popular	base	85.5	85.1	81.9	83.1	82.4	82.2
		ours	85.5	85.1	82.3	83.4	85.1	85.3
	Adversarial	base	79.1	79.9	74.8	77.9	74.7	76.9
		ours	79.5	80.1	75.3	78.2	78.2	79.9
GQA	Random	base	88.9	88.2	87.2	87.1	85.2	84.0
		ours	88.9	88.2	87.2	87.2	86.1	85.0
	Popular	base	84.1	84.1	78.6	80.4	78.7	78.5
		ours	84.2	84.1	78.8	80.4	81.0	80.5
	Adversarial	base	80.8	81.3	75.9	78.4	76.4	76.8
		ours	81.1	81.6	76.1	78.5	79.2	79.1

I Different Sampling Strategies

Tab. 12 presents an ablation study on sampling strategies (non-greedy vs. greedy). We follow the non-greedy sampling setting of VCD [26], where both top-p and temperature are set to 1. As shown, our method consistently improves performance across both sampling strategies.

Table 12: Ablation Study on Sampling Strategies on POPE MSCOCO Adversarial Dataset.

strategy	Method	LLaVA-v1.5		InstructBLIP		mPLUG-Owl2	
		Acc	F1	Acc	F1	Acc	F1
non-greedy	base	79.0 \pm 0.51	81.1 \pm 0.53	71.6 \pm 0.49	74.7 \pm 0.46	71.5 \pm 0.30	76.6 \pm 0.28
	ours	82.3 \pm 0.27	81.1 \pm 0.31	82.2 \pm 0.29	81.8 \pm 0.25	83.2 \pm 0.27	82.9 \pm 0.26
greedy	base	79.4	81.6	79.8	81.4	72.5	77.5
	ours	83.5	82.1	82.5	82.1	84.2	83.7

J Different Model Size

We evaluate our method on different model sizes, 7B and 13B, for LLaVA-v1.5 and InstructBLIP, as shown in Tab. 13. The results indicate consistent improvements across various model sizes. In each model series, the smaller model gets a larger performance boost. With our method, we can achieve high accuracy and detection rates with a smaller 7B model, outperforming a 13B model at its original performance level.

Table 13: Ablation Study on Model Size on LLaVA-QA90 Dataset.

Method	LLaVA-v1.5				InstructBLIP			
	7B		13B		7B		13B	
	Acc	Det	Acc	Det	Acc	Det	Acc	Det
base	3.23	3.54	4.78	4.2	3.84	4.07	5.67	4.88
ours	6.20	5.14	7.36	6.5	6.28	4.77	6.42	5.99

K Gradient Computation Details and Efficiency Ablation

Our method obtains gradients directly through PyTorch’s ‘torch.autograd.grad’ on input tokens, eliminating the need for manual derivations and facilitating straightforward reproduction. For comparison, we evaluate Integrated Gradients (IG) [11, 34, 21] using the SIG [11] implementation; Table 14 presents this ablation. In the table, “IG” denotes the SIG-based results, while “direct” refers to our torch.autograd.grad approach. Both methods yield comparable accuracy and F1-score, but the direct-gradient variant is substantially more efficient.

Table 14: Ablation Study on Gradient Methods on the POPE MSCOCO Adversarial Dataset

Methods		Accuracy	F1	Average Speed(ms)
MPLUG-Owl2	IG [11]	83.4	82.9	20335
	direct	84.2	83.7	385

L Norm Selection for Token Influence

To evaluate the impact of norm selection on token influence, we study L1 (Manhattan), L2 (Euclidean), and L_∞ (infinity) norms. The L1 norm highlights individual token contributions, while the L2 norm captures overall influence. The L_∞ norm focuses on the most dominant token or channel. Results in Tab. 15 show that the L1 norm achieves the best performance, aligning with our intuition that it effectively captures influence magnitude across tokens and channels. In contrast, the L2 norm, by emphasizing overall contribution, can obscure individual token effects, and the L_∞ norm, though capturing the strongest signal, fails to account for the broader token/channel influence.

Table 15: Norm Strategies on POPE MSCOCO Adversarial Dataset.

Norm	LLaVA-v1.5		InstructBLIP		mPLUG-Owl2	
	Acc	F1	Acc	F1	Acc	F1
L1	83.5	82.1	82.5	82.1	84.2	83.7
L2	83.2	81.9	79.5	79.6	83.2	82.9
L_∞	83.4	82.0	82.1	81.8	80.8	80.6

M Hyper parameter Study

Maximum α_m . To determine the optimal maximum amplification factor (α_m) and understand its impact on the model performance, we conducted a search over values from 1 to 6 using the LLaVA-v1.5 model on the POPE dataset for discriminative tasks. For open-ended generation tasks on a subset of the MSCOCO dataset following [10], we observed garbled text when α_m was set to 5; therefore, we limited our search to values from 1 to 4. As shown in Tab. 16 and Tab. 17, discriminative task on POPE is less sensitive to the value of α_m . The performance on the generative task gets improved while α_m increases but later drops. Therefore, in our experiments, the optimal maximum amplification factor (α_m) is set to 5 and 3 for discriminative and generation tasks, respectively.

Table 16: α_m Study For Discriminative Task On POPE [29] in MSCOCO Adversarial Setting.

Maximum α_m	1		2		3		4		5		6	
	Acc ↑	F1 ↑	Acc ↑	F1 ↑	Acc ↑	F1 ↑	Acc ↑	F1 ↑	Acc ↑	F1 ↑	Acc ↑	F1 ↑
LLaVA-v1.5	83.4	82.0	83.4	82.0	83.4	82.0	83.4	82.0	83.5	82.1	83.4	82.1

Table 17: Maximum α_m Study For Generation Task on the MSCOCO Subset.

Maximum α_m	1				2				3				4			
	$C_S \downarrow$	$C_I \downarrow$	$R \uparrow$	Len	$C_S \downarrow$	$C_I \downarrow$	$R \uparrow$	Len	$C_S \downarrow$	$C_I \downarrow$	$R \uparrow$	Len	$C_S \downarrow$	$C_I \downarrow$	$R \uparrow$	Len
LLaVA-v1.5	44.0	11.8	76.2	86.1	41.4	11.1	77.4	84.8	41.0	10.9	77.3	85.0	41.4	10.9	77.3	84.9

Early Stopping Threshold. To set the early stopping threshold properly, we conducted a search on a subset of the MSCOCO dataset subset following [10]. Recognizing that the visual influence ratio varies across models, we first analyze the sample-wise visual influence to identify an appropriate range for this study. By searching over the corresponding range, we show results in Tab. 18. These results demonstrate that varying the ES threshold primarily mediates the trade-off between recall and hallucination rate. Our goal is to have balanced recall (R) and instance-level hallucination (C_I), leading us to select thresholds of 7% for LLaVA-v1.5 and LLaVA-v1.6, 25% for InstructBLIP, 2.5% for mPLUG-Owl2 and 10% for InternVL2. We additionally ran an experiment to measure the ES activation rate using LLaVA-v1.5 with ES threshold 7%. As shown in Tab. 19, ES fires on only 8.7% of the test samples, and when it does, the generated responses are on average just 0.7 tokens shorter. This indicates that ES rarely, and only minimally, truncates outputs.

N Additional Implementation and Experimental Details

Noun tokens are identified using the spaCy library via its `en_core_web_sm` model. For experiments on the Amber dataset [44], we adopt the original data splits and evaluation metrics. In the MSCOCO [30] subset, we follow the data partitioning and evaluation protocol of Deng et al. [10], with splits available in their official repository. For the LLaVA-QA90 [32], MME [13] and POPE [29] datasets, our setup replicates that of Leng et al. [26] and use their provided scoring scripts for LLaVA-QA90. Experiments on MMBench [33], MM-Vet [49] follow the VLMEvalKit_InternVL2_5 repository. All comparison methods are executed using their official code; we only modify them to enforce greedy sampling and a uniform maximum generation length to align with our experimental settings.

Table 18: Early Stopping Threshold Study on the MSCOCO Subset

	LLaVA-v1.5				LLaVA-v1.6				InstructBLIP				mPLUG-Owl2				InternVL2			
	6%	7%	8%	9%	5%	7%	9%	11%	15%	20%	25%	30%	2%	2.5%	3%	3.5%	8%	10%	12%	14%
C_S	45.6	41.0	36.6	31.4	29.0	26.0	23.0	17.8	52.6	51.4	47.4	36.0	51.8	45.0	41.2	41.0	37.0	35.2	34.6	32.9
C_I	11.5	10.9	10.2	10.2	8.5	8.1	7.8	7.5	15.0	14.3	13.4	11.7	13.7	12.4	11.0	11.0	8.6	8.1	8.0	7.9
R	79.7	77.3	75.2	70.8	68.5	63.0	58.8	53.0	75.1	74.4	72.3	68.8	77.7	74.9	73.8	73.5	65.8	65.4	65.4	64.0
L_{en}	92.0	85.0	75.4	63.9	119.1	101.8	81.1	62.7	107.9	103.4	93.9	74.3	89.1	83.5	78.9	77.8	180.4	175.5	170.6	162.2

Table 19: Activation Rate of the Early Stopping on the MSCOCO Subset

	Methods	Activate Percentage	Average Length
LLaVA-v1.5 (7%)	base	-	85.1
	ours	8.7%	84.4

O Question Category Results on the AMBER Dataset

We report discriminative results across different question categories in Tab. 20. Our method improves performance in nearly all categories across all MLLMs. The improvement in InternVL2’s object existence is minor, likely due to its already high visual influence ratio. For LLaVA-v1.5 and mPLUG-Owl2, which have lower original visual influence ratios, our method achieves more substantial gains in existence, attribute, and state categories.

Table 20: Results on the Question Categories of Discriminative Task on AMBER Dataset.

Category	Metric	InstructBLIP		LLaVA-v1.5		LLaVA-v1.6		mPLUG-Owl2		Intern-VL2	
		base	ours	base	ours	base	ours	base	ours	base	ours
Existence	acc	70.0	79.8	70.8	93.2	92.9	93.0	75.2	89.9	90.6	90.6
	P	100.0	100.0	100.0	100.0	100.0	100.0	100.0	100.0	100.0	100.0
	R	70.0	79.8	70.8	93.2	92.9	93.0	75.2	89.9	90.6	90.6
	F1	82.3	88.7	82.9	96.4	96.3	96.3	85.8	94.6	95.0	95.0
Attribute	acc	71.9	78.3	72.3	76.1	75.2	77.1	73.9	78.2	82.3	82.6
	P	76.0	81.7	87.3	74.0	74.6	76.4	86.0	76.9	80.9	80.9
	R	64.3	73.0	52.2	82.7	83.0	83.9	57.1	81.8	84.7	85.2
	F1	69.7	77.1	65.3	78.1	78.5	80.0	68.6	79.3	82.8	83.0
State	acc	73.4	76.4	68.2	73.3	78.6	75.2	70.5	77.9	81.2	81.2
	P	75.1	77.1	86.2	70.3	78.6	74.7	84.9	75.5	79.1	78.7
	R	70.6	75.3	43.3	82.0	78.5	82.9	49.8	83.1	84.8	85.5
	F1	72.8	76.2	57.6	75.7	78.5	78.6	62.8	79.1	81.8	82.0
Number	acc	65.4	80.6	75.0	80.1	80.1	80.2	77.8	76.5	82.6	83.3
	P	75.4	93.1	86.9	79.1	79.2	78.6	86.0	77.0	83.0	84.0
	R	45.8	66.2	59.5	82.4	81.7	84.4	66.9	77.0	82.0	82.3
	F1	57.0	77.4	70.6	80.7	80.4	81.4	75.3	77.0	82.5	83.1
Action	acc	79.7	83.7	83.6	82.3	81.9	80.4	84.0	84.1	88.4	88.6
	P	82.5	88.5	92.9	85.9	79.4	81.2	90.9	85.9	86.5	86.8
	R	75.3	77.5	72.7	87.4	86.0	88.6	75.5	85.9	90.9	91.2
	F1	78.7	82.6	81.6	86.6	82.6	84.7	82.5	85.9	88.6	88.9
Relation	acc	62.7	71.9	71.8	61.5	64.5	65.7	70.5	76.9	72.1	77.0
	P	56.2	64.0	65.9	51.9	54.0	56.6	61.0	67.9	60.0	65.1
	R	48.6	73.4	66.3	97.7	95.1	87.2	79.5	83.9	98.3	95.6
	F1	52.1	68.4	66.1	67.8	68.9	68.6	69.0	75.1	74.5	77.5

P Confidence and Visual Influence

Low confidence often signals potential failure modes in base MLLMs. Here, we demonstrate that our method not only improves accuracy but also increases model confidence. It remains effective even in low-confidence regions for three reasons: 1) We aggregate token gradients at the component level

(Eq. 5) rather than using individual token gradients which yields robustness against local gradient noise. 2) We adjust influence towards visual tokens which consistently reduces the hallucination likelihood; 3) Empirically, low model confidence does not correlate with noisy gradients. In our experiments, pretrained MLLMs usually maintain meaningful gradient signals even at low confidence levels. Fig. 6 shows an example where the baseline model mPLUG-Owl2 exhibits low confidence in hallucinated predictions and near-zero confidence in the initial predictions for ‘forks’ and ‘mug’. With GACD, prediction confidence increases alongside the visual influence ratio, with the minimum confidence rising to over 30%.

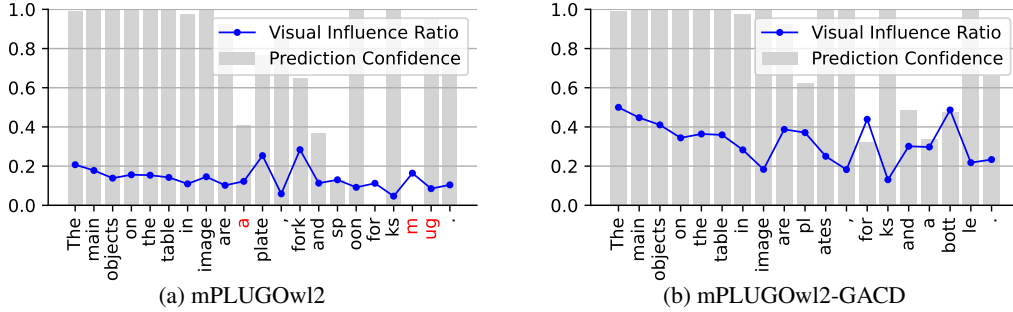


Figure 6: Comparison of prediction confidence with and without GACD. (a) Without GACD, mPLUGOwl2 exhibits low confidence in **hallucinated predictions** and near-zero confidence in the initial predictions for ‘forks’ and ‘mug’. (b) With GACD, mPLUGOwl2’s confidence increases alongside the **visual influence ratio**, effectively mitigating hallucinations.

Q Qualitative Example on Occluded Images

We include a qualitative example in Fig. 7, where a sedan and a building are partially occluded by a white truck, our method prevents the baseline model from hallucinating of persons and vehicles behind the occluding object. This demonstrates our method remains effective on images consisting of occlusions. Image caption w/o Ours: The image features a white truck parked on a city street, with



Image caption w/o Ours: The image features a white truck parked on a city street, with graffiti covering its side. The truck is positioned near a crosswalk, and there are several other vehicles in the scene, including a car and a bus. In addition to the vehicles, there are a few people walking around the area.

Image caption w Ours: The image features a large white truck parked on a city street, with graffiti covering its side. The truck is positioned near a crosswalk, and there is another vehicle visible in the background. Additionally, there are buildings in the scene, suggesting an urban setting.

Figure 7: Example of our method applied to an occluded image.

graffiti covering its side. The truck is positioned near a crosswalk, and there are several other vehicles in the scene, including a car and a bus. In addition to the vehicles, there are a few people walking around the area. Image caption w Ours: The image features a large white truck parked on a city street, with graffiti covering its side. The truck is positioned near a crosswalk, and there is another vehicle visible in the background. Additionally, there are buildings in the scene, suggesting an urban setting.

R Computational Cost

In this section, we analyze the computational cost of the proposed method. Typically, gradient computation adds an overhead equivalent to 1–2 times the cost of a forward pass. As a result, our approach increases the overall computational cost by up to five times compared to the baseline while remaining significantly lower than fine-tuning-based methods. Notably, contrastive logits generation involves only a small number of visual tokens, helping to reduce the actual runtime cost.

S Influence Ratio in Image Caption

We further visualize the influence ratio in the image captioning task. Fig. 8 shows that in the baseline LLaVA-v1.5, the influence gap between previous output tokens and visual tokens widens as more tokens are generated. However, GACD effectively narrows this gap, preventing visual information from being forgotten and thereby reducing hallucinations.



LLaVA: The image features a black dog lying on the floor in a kitchen, resting comfortably on a tiled surface. The dog is positioned near a bowl, possibly **enjoying a meal or a snack**. In the kitchen, there are several items scattered around. **A bottle can be seen on the left side of the dog, while a cup is located closer to the center. A spoon is placed near the right side of the dog, and a bowl is situated on the right side of the scene.**

LLaVA-VA: The image features a black dog lying on the floor of a kitchen, resting comfortably on a tile floor. The dog is positioned near a bowl, a toy, and a bag of cat food. The bowl is placed on the floor, while the toy is located closer to the dog.

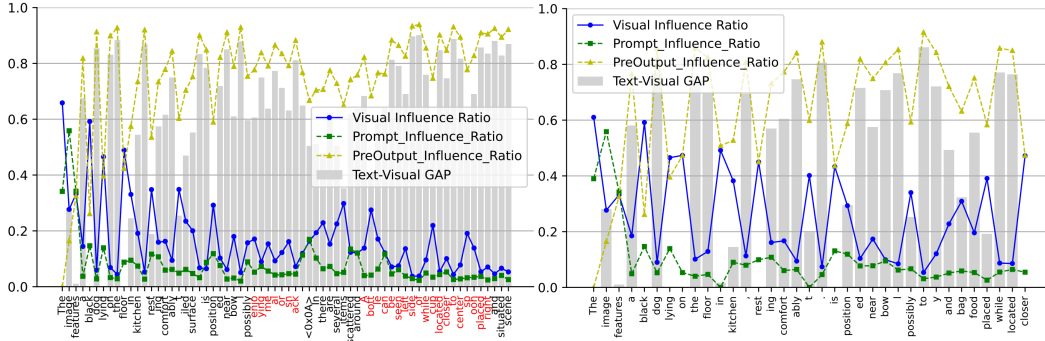


Figure 8: Comparison of influence ratios across predicted tokens with and without GACD. (Left) Without GACD, the influence gap between **previous output tokens** and **visual tokens** widens as more tokens are generated. (Right) With GACD, the gap is periodically narrowed to nearly zero, mitigating this trend and reducing hallucination.

T Influence Ratio in VQA

Fig. 9 illustrates the visual influence ratio across outputs in VQA tasks, comparing baseline predictions with those obtained after applying GACD. The results confirm that text tokens dominate influence across MLLMs, including InternVL2, which exhibits a relatively high visual influence ratio. As shown in Fig. 3 of the main paper, the overall 60%–100% visual influence ratio across the POPE dataset suggests that visual inputs predominantly determine object existence in VQA tasks. GACD enhances visual influence, effectively balancing text-visual bias. Furthermore, the visualization on InternVL2 demonstrates that the co-occurrence hallucination ‘knife’ persists despite a high visual influence. GACD successfully eliminates this co-occurrence hallucination.

U Limitations and Future Work

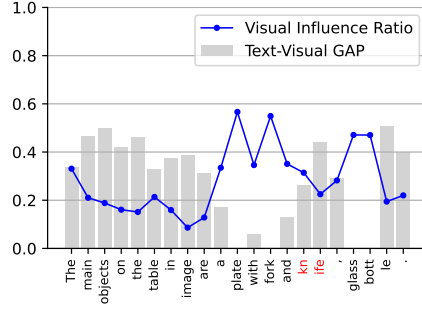
Our method is limited to white-box MLLMs, as it requires access to gradients. Its effectiveness depends on the baseline MLLM’s original visual influence ratio, and the importance of visual information. As a post-processing technique, our method does not involve model training. In future work, we aim to explore how insights from GACD can guide and improve training strategies for enhanced visual perception in MLLMs.

V Broader Impacts

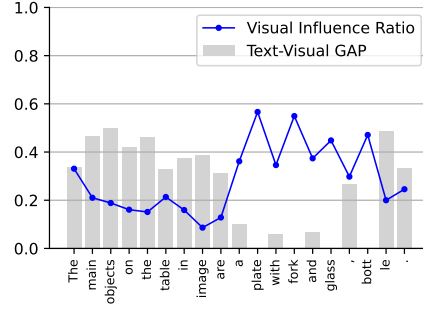
Our method enhances the factual reliability of multi-modal language models, not only for vision–language tasks but also for modalities such as video and audio, by mitigating hallucinations at inference time. This improvement has several positive societal implications: it can make systems for visual question answering, assistive technologies for the visually impaired, and automated image captioning more dependable, thereby increasing user trust and safety; it can power educational tools that generate accurate descriptions of complex diagrams or historical media, benefiting learners and instructors; and in critical domains such as medical imaging or remote sensing, it can reduce spurious outputs and support more robust decision-making. Conversely, if deployed within surveillance or facial-recognition systems, stronger multi-modal grounding could facilitate more intrusive inferences about individuals from visual data, exacerbating privacy risks.



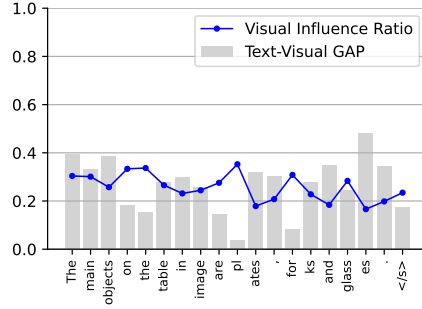
(a) What are the main objects on the table in the image?



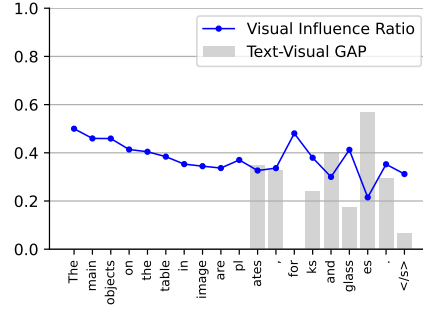
(b) LLaVA v1.5



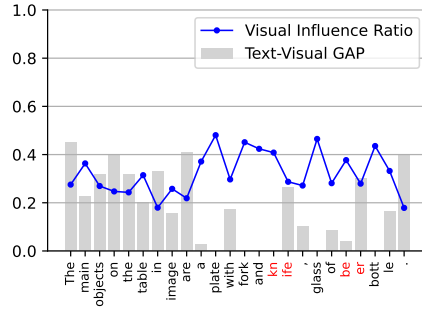
(c) LLaVA v1.5-GACD



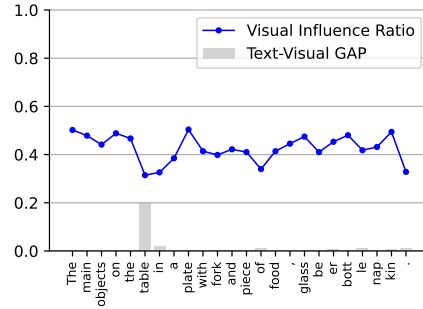
(d) InstructBLIP



(e) InstructBLIP-GACD



(f) InternVL2



(g) InternVL2-GACD

Figure 9: Influence Ratio across Predicted Tokens in VQA: (left) Baseline predictions; (right) Predictions with GACD. GACD effectively mitigate Text-Visual GAP, balancing text-visual bias. (f) The original InternVL2 shows a dominant visual influence ratio at the hallucinated prediction ‘knife’, indicating a co-occurrence bias that remains unaddressed even with dominant visual influence. (g) GACD successfully eliminates co-occurrence hallucinations, including ‘knife’.